IDENTIFICATION OF UNDERWATER VEHICLE HYDRODYNAMIC COEFFICIENTS USING FREE DECAY TESTS

Andrew Ross * **Thor I. Fossen** *,** **Tor Arne Johansen** **

* *Centre for Ships and Ocean Structures*
Norwegian University of Science and Technolog
NO-7491 Trondheim, Norway
** *Department of Engineering Cybernetics*
Norwegian University of Science and Technology
NO-7491 Trondheim, Norway
E-mail: andrew.ross@marin.ntnu.no, tif@itk.ntnu.no,
tor.arne.johansen@itk.ntnu.no

Abstract: A new method is proposed for the experimental determination of the longitudinal and lateral hydrodynamic coefficients of a low-speed UUV. The technique presented is a development of the classical free-decay test. A body is excited with a mechanism of springs, and system identification techniques are carried out on measured data, with the intention of evaluating the added mass and linear damping of the body in decoupled longitudinal and lateral models. Simulated results are presented in order to estimate the potential accuracy of these new methods.

Keywords: Low-speed underwater vehicles, system identification, free decay test, digital differentiators

INTRODUCTION

In recent years there has been an ever increasing number of applications for unmanned underwater vehicles (UUV) in various tasks, for instance in surveying and exploration, or in missions such as the positioning of underwater laboratories (Aguiar 1997). Improvements in the evaluation of the hydrodynamic models of UUV's result in more effective control system implementation, leading to increased capability and performance in underwater operations. The efficient identification of hydrodynamic coefficients is a task which is difficult and oftentimes expensive to carry out, with many examples of how to measure or estimate them. For example, the use of towing tanks in a marine laboratory (Aage 1994) is well-established, as is the hydrodynamic modelling of underwater vehicles in computational fluid dynamics programs such as WAMIT. System identification techniques have found valuable application, for instance in Smallwood and Whitcomb (2003), Caccia *et al.* (2000), A.T Morrison III (1993), Blanke (1997).

Previous work has generally been limited by only identifying parameters in a single degree-of-freedom (DOF). For a full treatise on the classical free decay test see Faltinsen (1990). This paper advances in the area of identification by proceeding to apply techniques of system identification to a multiple-DOF model. The experiments under investigation are longitudinal free decay tests, but the results are valid for the lateral mode as well. Under investigation is whether, and to what accuracy, various hydrodynamic parameters might be estimated. Digital signal processing is applied to generate the body velocities and accelerations from only position, and parameters are estimated using linear regression.

1. UNDERWATER VEHICLE MODEL

1.1 Dynamics

This section describes the underwater vehicle dynamics, i.e. the kinematic and kinetic equations of motion.

1.1.1. Kinematics The kinematic model used is that of (Fossen 2002):

$$\dot{\eta} = J(\eta)\nu \tag{1}$$

Where $\eta = [x, y, z, \phi, \theta, \psi]^\top$ is the vehicle's generalised position in an inertial frame, $\nu = [u, v, w, p, q, r]^\top$ is the UUV's generalised velocity in the body frame, and $J(\eta) \in R^{6\times6}$ is the velocity transformation matrix from the body to the inertial frame.

1.1.2. Kinetics The dynamic equations of motion can be represented as a high-speed model for maneuvering or a low-speed model for station-keeping and low-speed maneuvering as detailed in Fossen (2002).

High-speed model: The nonlinear high-speed model is written:

$$(M_{RB} + M_A)\dot{\nu} + (C_{RB}(\nu) + C_A(\nu))\nu + D(\nu)\nu + g(\eta) = \tau \tag{2}$$

where $M_{RB} \in R^{6\times6}$ and $M_A \in R^{6\times6}$ are system inertia matrices for the rigid body and hydrodynamic added mass, respectively, $\mathbf{C}_{RB} \in \mathbf{R}^{6\times6}$ and $C_A \in R^{6\times6}$ are the Coriolis-centripetal terms corresponding to these, $D(\nu) \in R^{6\times6}$ is a nonlinear damping matrix, $g(\eta) \in R^{6\times1}$ is a vector of generalised gravity and buoyancy forces, and $\tau \in R^6$ is the generalised force applied

Low-speed model: To derive the low-speed model, it is assumed that the Coriolis-centripetal forces and non-linear damping are negligible, giving:

$$C(\nu)\nu \approx 0 \tag{3}$$

$$D(\nu)\nu \approx N\nu \tag{4}$$

where $N \in R^{6\times6}$ is a matrix of linear damping coefficients. Consequently (2) takes the form:

$$M\dot{\nu} + N\nu + g(\eta) = \tau \tag{5}$$

where

$$M = M_{RB} + M_A \tag{6}$$

Spring forces due to the attachment device: In the free decay experiments, it is assumed that the vehicle is attached to its surroundings using linear springs (see Figure 2) described by:

$$\tau = -K\eta \tag{7}$$

where $K \in R^{6\times6}$ is the spring stiffness matrix and $\tau \in R^6$ is the generalised force applied. The control forces (thrust) are set to zero in the experiments.

1.2 Decoupling into Lateral and Longitudinal Modes

The 6 DOF equations of motion can in many cases be divided into two non-interacting (or lightly interacting) subsystems. This decomposition is good for starboard-port symmetrical slender bodies, that is, bodies with large length/width ratios (Gertler and Hagen 1967, Feldman 1979, Tinker 1982).

- **Longitudinal subsystem:** states u, w, q, x, z, θ
- **Lateral subsystem:** states v, p, r, y, ϕ, ψ

The system inertia matrix can then be partitioned according to (Fossen 2002):

$$M_{\text{lon}} = \begin{bmatrix} m_{11} & m_{13} & m_{15} \\ m_{31} & m_{33} & m_{35} \\ m_{51} & m_{53} & m_{55} \end{bmatrix} M_{\text{lat}} = \begin{bmatrix} m_{22} & m_{24} & m_{26} \\ m_{42} & m_{44} & m_{46} \\ m_{62} & m_{64} & m_{66} \end{bmatrix}$$

1.2.1. Longitudinal Subsystem Without loss of generality, we will assume that the lateral states v, p, r, ϕ are small, the weight $W = mg$ is equal to the buoyancy force B, and that the center of gravity coincides with the center of buoyancy in the x-direction, i.e. $x_G = x_B$, etc. Then the kinematic model in *surge, heave*, and *pitch* can be expressed according to (Fossen 2002):

$$\dot{\eta}_{\text{lon}} = J_{\text{lon}}(\eta_{\text{lon}})\nu_{\text{lon}} \tag{8}$$

with:

$$J_{\text{lon}}(\eta_{\text{lon}}) = \begin{bmatrix} \cos\theta & \sin\theta & 0 \\ -\sin\theta & \cos\theta & 0 \\ 0 & 0 & 1 \end{bmatrix} \tag{9}$$

where $\eta_{\text{lon}} = [x, z, \theta]^\top$ and $\nu_{\text{lon}} = [u, w, q]^\top$. The kinetics takes the form:

$$M_{\text{lon}}\dot{\nu}_{\text{lon}} + N_{\text{lon}}\nu_{\text{lon}} + g(\eta_{\text{lon}}) = -K_{\text{lon}}\eta_{\text{lon}} \tag{10}$$

where

$$M_{\text{lon}} = \begin{bmatrix} m - X_{\dot{u}} & -X_{\dot{w}} & mz_g - X_{\dot{q}} \\ -X_{\dot{w}} & m - Z_{\dot{w}} & -mx_g - Z_{\dot{q}} \\ mz_g - X_{\dot{q}} & -mx_g - Z_{\dot{q}} & I_y - M_{\dot{q}} \end{bmatrix}$$

$$N_{\text{lon}} = \begin{bmatrix} -X_u & -X_w & -X_q \\ -Z_u & -Z_w & -Z_q \\ -M_u & -M_w & -M_q \end{bmatrix}$$

$$g(\eta_{\text{lon}}) = \begin{bmatrix} 0 \\ 0 \\ WBG_z \sin\theta \end{bmatrix}$$

1.2.1.1. Longitudinal Spring Stiffness Matrix At rest $\dot{\nu}_{\text{lon}} = \nu_{\text{lon}} = 0$ the spring forces $K_{\text{lon}}\eta_{\text{lon}}$ must balance out the gravitational and buoyancy forces term, $g_{\text{lon}}(\eta_{\text{lon}})$, that is:

$$g_{\text{lon}}(\eta_{\text{lon}}) + K_{\text{lon}}\eta_{\text{lon}} = 0 \tag{11}$$

For the experimental set-up depicted in Figure (2) where k_1 and k_2 are the stiffness values of the respective springs, the K_{lon} matrix becomes:

$$K_{\text{lon}} = \begin{bmatrix} k_1 + k_2 & 0 & 0 \\ 0 & k_1 + k_2 & 0 \\ k_1 r_{z1} + k_2 r_{z2} & k_1 r_{x1} + k_2 r_{x2} & 0 \end{bmatrix} \tag{12}$$

where (r_{1x}, r_{1z}) and (r_{2x}, r_{2z}) are the locations of the spring attachments on the UUV relative to the centre of gravity.

1.2.2. Lateral Subsystem Assume that the lateral states longitudinal states u, w, p, r, ϕ and θ, the weight $W = mg$ is equal to the buoyancy force B, and that the center of gravity coincides with the center of buoyancy in the x-direction, i.e. $x_G = x_B$, etc. Then the kinematic model in *sway, roll*, and *yaw* can be expressed according to (Fossen 2002):

$$\dot{\eta}_{\text{lat}} = \nu_{\text{lat}} \tag{13}$$

where $\eta_{\text{lat}} = [y, \phi, \psi]^\top$ and $\nu_{\text{lat}} = [v, p, r]^\top$. The kinetics takes the form:

$$M_{\text{lat}}\dot{\nu}_{\text{lat}} + N_{\text{lat}}\nu_{\text{lat}} + g_{\text{lat}}(\eta_{\text{lat}}) = -K_{\text{lat}}\eta_{\text{lat}} \tag{14}$$

where

$$M_{\text{lat}} = \begin{bmatrix} m - Y_{\dot{v}} & -mz_g - Y_{\dot{p}} & mx_g - Y_{\dot{r}} \\ -mz_g - Y_{\dot{p}} & I_x - K_{\dot{p}} & -I_{zx} - K_{\dot{r}} \\ mx_g - Y_{\dot{r}} & -I_{zx} - K_{\dot{r}} & I_z - N_{\dot{r}} \end{bmatrix}$$

$$N_{\text{lat}} = \begin{bmatrix} -Y_v & -Y_p & -Y_r \\ -M_v & -M_p & -M_r \\ -N_v & -N_p & -N_r \end{bmatrix}$$

$$g_{\text{lat}}(\eta_{\text{lat}}) = \begin{bmatrix} 0 \\ WBG_z \sin\phi \\ 0 \end{bmatrix}$$

2. FREE DECAY TEST

The MIMO free decay test is performed according to flow chart in Figure 1.

2.1 State Measurements

For the experiments envisaged in this paper, an underwater camera system is to be used. This system works by identifying pre-determined markings on the UUV, and measures at 20 Hz. Using cameras offers measurements of only the generalised position, η, and therefore suitable methods must be applied in order to generate the estimates of the states ν and $\dot{\nu}$.

2.1.1. Zero Phase Differentiation In order to reduce system complexity and cost, filtering techniques are applied to generate the unknown derivatives. In this paper a differentiator filter is applied twice in order to generate the body velocities and accelerations according to the kinematics formula (1) we can write:

$$\eta_m = \eta + w \tag{15}$$

$$\hat{\nu} = J^{-1}(\eta_m)\Lambda(\eta_m) \tag{16}$$

$$\dot{\hat{\nu}} = \Lambda(\hat{\nu}) \tag{17}$$

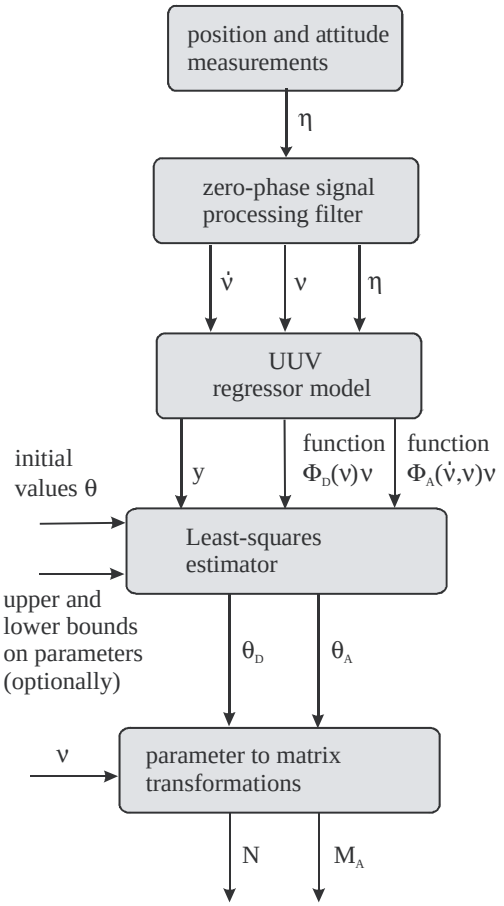

Fig. 1. Free Decay Flow Diagram

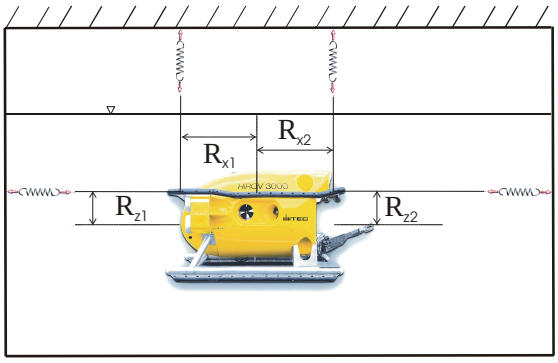

Fig. 2. Experimental set-up for longitudinal identification showing the UUV attached by 4 springs.

where $\Lambda(x)$ is a differentiation filter producing an estimate $\dot{x}$, and w is an error term, assumed to be zero-mean white noise, which enters the system through the measurements η_m of η. The differentiator is a *least squares band-limited FIR* filter of order of 301 (Oppenheim and Schafer 1989) and was generated using the Matlab program *FDATool* from the filter toolbox. Thus the filter's magnitude drops off quickly at 2Hz, and so also low-pass filters the outputs and does not differentiate high frequency noise. As the filtering is not required to be achieved in real-time, and the filter itself has linear phase properties, the phase lag is trivial to compensate for by simply time-shifting the output by -150 samples.

3. SYSTEM IDENTIFICATION

The task of system identification is essentially matching a model of some form to experimental data, in order that the model explains, in some fashion, the experimental data.

$$\min_{\theta} V = \frac{1}{2}\int_0^t (y - \Phi(\dot{\nu},\nu)\theta)^\top (y - \Phi(\dot{\nu},\nu)\theta)\, d\tau \tag{18}$$

where y, $\Phi(\dot{\nu},\nu)$ and θ are defined in their derivation at (19), and V is a quadratic cost function of these variables. Since the problem is linear, the optimisation problem is solved using the standard least squares solution.

3.1 Parametric Form

The dynamic model of the vehicle can be transformed to a linear parametric form:

$$y = \Phi^T(\dot{\nu},\nu)\theta \tag{19}$$

in which y is a vector consisting of measured or calculable data, $\Phi(\dot{\nu},\nu)$ is the regression matrix, and θ is the unknown parameter vector. Assume that the rigid-body system inertia matrix M_{RB} and gravity/buoyancy vector $g(\eta)$ is known while added mass M_A and damping N are unknown. This is the usual case when modeling underwater vehicles. Consider the free decay test (low-speed) model:

$$(M_{RB} + M_A)\dot{\nu} + N\nu + g(\eta) = -K\eta \tag{20}$$

which can be written:

$$M_A\dot{\nu} + N\nu = y \tag{21}$$

where the signal y is computed from the measurements and *known parameters* K, M_{RB}, and $g(\eta)$ according to:

$$y = -K\eta - M_{RB}\dot{\nu} - g(\eta) \tag{22}$$

The *regressor matrix* and *parameter vector* are obtained from:

$$\Phi_M^T(\dot{\nu},\nu)\theta_M := M_A\dot{\nu} \tag{23}$$
$$\Phi_N^T(\dot{\nu},\nu)\theta_N := N\nu \tag{24}$$

such that:

$$\Phi^T(\dot{\nu},\nu) = [\Phi_M^T(\dot{\nu}), \Phi_N^T(\nu)], \quad \theta = \begin{bmatrix}\theta_M \\ \theta_N\end{bmatrix} \tag{25}$$

3.2 Case Study: Longitudinal Mode

For the longitudinal mode, we get:

$$y_{\text{lon}} = -K_{\text{lon}}\eta_{\text{lon}} - M_{RB}\dot{\nu}_{\text{lon}} - g_{\text{lon}}(\eta_{\text{lon}}) \tag{26}$$

The regressor matrices take the form:

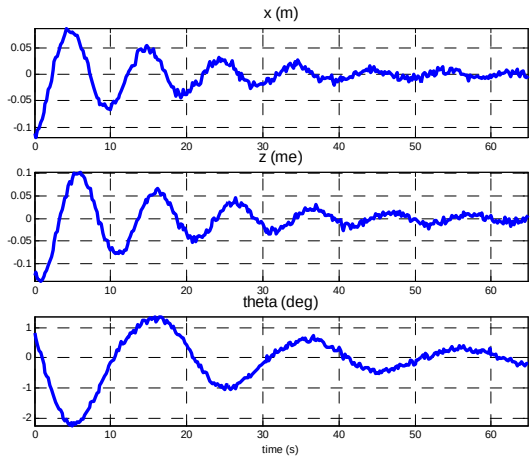

Fig. 3. Free Decay Test Showing Position (x, z) and pitch angle θ versus time. The UUV is moved out of its equilibrium at $(0, 0)$ and released

$$\Phi_M^T(\dot{\nu}_{\text{lon}}) = -\begin{bmatrix} \dot{u} & \dot{w} & \dot{q} & 0 & 0 & 0 & 0 \\ 0 & \dot{u} & 0 & \dot{w} & \dot{q} & 0 & 0 \\ 0 & 0 & \dot{u} & 0 & 0 & \dot{w} & \dot{q} \end{bmatrix} \tag{27}$$

$$\Phi_N^T(\nu_{\text{lon}}) = -\begin{bmatrix} u & w & q & 0 & 0 & 0 & 0 & 0 & 0 \\ 0 & 0 & 0 & u & w & q & 0 & 0 & 0 \\ 0 & 0 & 0 & 0 & 0 & 0 & u & w & q \end{bmatrix} \tag{28}$$

and the corresponding parameter vectors are:

$$\theta_M = [X_{\dot{u}}, X_{\dot{w}}, X_{\dot{q}}, Z_{\dot{w}}, Z_{\dot{q}}, M_{\dot{q}}]^\top \tag{29}$$
$$\theta_N = [X_u, X_w, X_q, Z_u, Z_w, Z_q, M_u, M_w, M_q]^\top \tag{30}$$

where we have assumed that $M_A = M_A^\top$ while $N \neq N^\top$.

4. SIMULATIONS AND RESULTS

The longitudinal system was implemented in Simulink for an UUV given by the following parameters:

$$M_{RB} = \begin{bmatrix} 1000 & 0 & 200 \\ 0 & 1000 & 0 \\ 200 & 0 & 11000 \end{bmatrix} \tag{31}$$

$$M_A = \begin{bmatrix} 1000 & 0 & 100 \\ 0 & 1100 & 80 \\ 100 & 80 & 9000 \end{bmatrix} \tag{32}$$

$$N = \begin{bmatrix} 210 & 20 & 30 \\ 25 & 200 & 70 \\ 15 & 33 & 1500 \end{bmatrix} \tag{33}$$

The the spring coefficients were set to $k_1 = 300$, $k_2 = 500$.

Figure 6 shows a phase portrait of the test, with the body starting at $(0.5, 0.5)$ and spiraling inwards, and figure 3 shows the states during the same simulation. Figure 4 shows the generated states w and $\dot{w}$, with close correlation, after a short transient, being evident. During identification, the transient data is discarded.

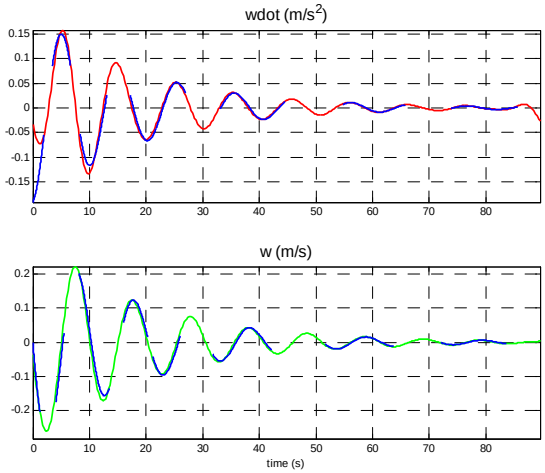

Fig. 4. Free decay test: plot showing the computed derivatives w and $\dot{w}$ and their true values using the zero-phase differentiator filter.

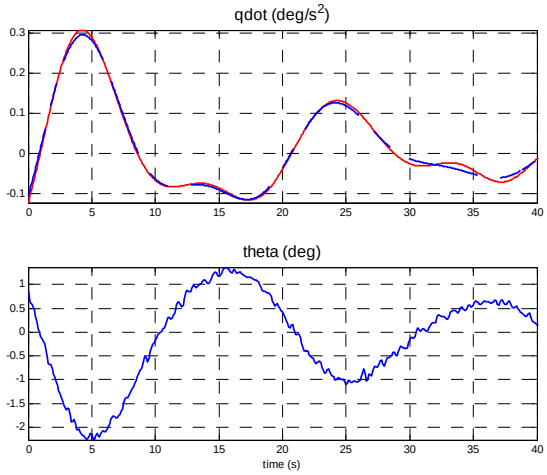

Fig. 5. Measured Pitch Angle (θ_m) with $\dot{q}$ and its estimate $\hat{\dot{q}}$

By examining $\dot{q}$ in Figure 5, the closeness of $\hat{\dot{q}}$ to the actual state $\dot{q}$ is evident, and the lack of differentiated noise from θ is also clear. Firstly the system identification procedure was carried out using perfect state knowledge, that is without applying the filtering or adding noise, with the result that the parameter estimates corresponded exactly with the actual parameters. Carrying out the identification using the realistic state estimates based solely on the noisy measurements of η led to the results shown in Table 1.

The estimates of the diagonal elements in M_A and N are generally very strong, especially that of $M_{\dot{q}}$ and M_q. Overall, the added mass matrix is very well modelled. The estimates of some off-diagonal elements in N are to a lower quality, notably Z_u and Z_q. Other off-diagonal elements are estimated extremely well, with X_w and X_q being particularly well evaluated. The added mass matrix is more accurately modelled than the damping matrix primarily due to prior knowledge of its structure, such as the assumption of symmetry.

Hydrodynamic Derivative	Real	Estimate
$X_{\dot{u}}$	1000	928.5
$X_{\dot{q}}/Z_{\dot{u}}$	200	213
$Z_{\dot{w}}$	1100	1031
$Z_{\dot{q}}/M_{\dot{w}}$	80	92.4
$M_{\dot{q}}$	9000	8981
X_u	210	234.9
X_w	20	21.3
X_q	30	32.7
Z_u	25	49.5
Z_w	200	208.7
Z_q	70	41.5
M_u	15	29.9
M_w	33	29.5
M_q	1500	1483.8

Table 1. Hydrodynamic derivatives and their estimates.

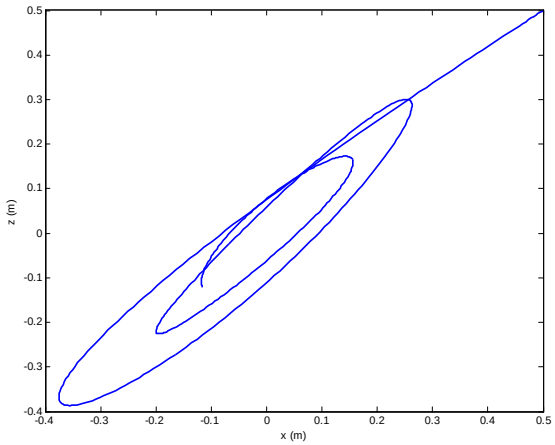

Fig. 6. Free decay test: side view showing the positions (x, z). Notice that the vehicle is only moving approximately 0.50 m in each direction.

5. CONCLUSIONS

The new methods are presented, with simulated experimental results for the longitudinal model, demonstrating the combination of simulation with signal processing and system identification. The implications of the paper must be verified through actual experimentation to gain a clearer picture of the applicability and usefulness of the methods presented. The fact that the evaluation process converges to the correct parameters with full state knowledge implies identifiability, and so the problem is primarily one of achieving effective state measurement. The penalty of using signal processing method is that, although cheap, errors arise in state measurement, leading to the innacuracies noted in the previous section. The addition of an inertial measurement unit entirely reverses the advantages and disadvantages, in that this setup would be expensive but far more accurate. That stated, if future experiments match the simulations presented here, it can

be expected that a system leading on from this will be both useful and versatile in the derivation of the hydrodynamic coefficients of low-speed UUV's.

6. ACKNOWLEDGEMENT

The authors are grateful to the Research Council of Norway for financial support through the Centre for Ships and Ocean Structures (CESOS) and the Strategic University Program on Computational Methods in Nonlinear Motion Control.

REFERENCES

Aage, C., Wagner Smitt L. (1994). Hydrodynamics manoeuvrability data of a flatfish type AUV. In: *Oceans*. Vol. 3. pp. 425–430.

Aguiar, A., Pascoal A. (1997). Modelling and control of an autonomous underwater shuttle for the transport of benthic laboratories. In: *OCEANS*. Vol. 2. pp. 888–895.

A.T Morrison III, D.R. Yoerger (1993). Determination of the hydrodynamic parameters of an underwater vehicle during small scale, nonuniform, 1-dimensional translation. *OCEANS* **2**, 277–282.

Blanke, M., Tiano A (1997). Multivariable identification of ship steering and roll motions. *Transactions of the Institute of Measurement and Control* **19**(2), 62–77.

Caccia, M., G. Indiveri and G. Veruggio (2000). Modelling and identification of open-frame variable configuration unmanned underwater vehicles. *IEEE Journal of Oceanic Engineering* **25**(2), 227–240.

Faltinsen, O. M. (1990). *Sea Loads on Ships and Offshore Structures*. Cambridge University Press.

Feldman, J. (1979). DTMSRDC Revised Standard Submarine Equations of Motion. Technical Report DTNSRDC-SPD-0393-09. Naval Ship Research and Development Center. Washington D.C.

Fossen, T. I. (2002). *Marine Control Systems: Guidance, Navigation and Control of Ships, Rigs and Underwater Vehicles*. Marine Cybernetics AS. Trondheim, Norway. ISBN 82-92356-00-2.

Gertler, M. and G. R. Hagen (1967). Standard Equations of Motion for Submarine Simulation. Technical Report DTMB-2510. Naval Ship Research and Development Center. Washington D.C.

Oppenheim, A.V and R.W Schafer (1989). *Discrete-Time Signal Processing*. Prentice-Hall, Englewood Cliffs, NJ.

Smallwood, D.A and L.L Whitcomb (2003). Adaptive identification of dynamically positioned underwater robotic vehicles. *IEEE Transactions on Control Systems Technology* **11**(4), 505–515.

Tinker, S. J. (1982). Identification of Submarine Dynamics from Free-Model Test. In: *Proceedings of the DRG Seminar*. The Netherlands.